



## Elaboration and characterization of novel PES/nanocomposites mixed matrix membranes

Imen Ben Belgacem<sup>a</sup>, Hazem Bouhamed<sup>b</sup>, Patrick Loulergue<sup>c</sup>, Anthony Szymczyk<sup>c</sup>, Sabeur Khemakhem<sup>a,\*</sup>

<sup>a</sup>Laboratoire Sciences des Matériaux et Environnement, Université de Sfax, Faculté des Sciences de Sfax, Route de Soukra Km 4, 3038 Sfax, Tunisia, emails: khemakhem\_sabeur@yahoo.fr (S. Khemakhem), imen\_ben\_belgacem@yahoo.fr (I.B. Belgacem)

<sup>b</sup>Laboratory of Industrial Chemistry, National School of Engineering, Sfax University, Box: 1173, Sfax 3038, Tunisia, email: hazem.bouhamed@gmail.com

<sup>c</sup>Université de Rennes, CNRS, ISCR - UMR 6226, F-35000 Rennes, France, emails: patrick.loulergue.1@univ-rennes1.fr (P. Loulergue), anthony.szymczyk@univ-rennes1.fr (A. Szymczyk)

Received 18 April 2019; Accepted 27 July 2019

### ABSTRACT

In this study, novel polyethersulfone (PES) membranes were blended for the first time with nanocomposites from the system (ZnO-TiO<sub>2</sub>-SiO<sub>2</sub>-CeO<sub>2</sub>). The obtained composite membranes by wet-phase inversion method were subsequently characterized and finally used for the filtration of lysozyme solutions. The incorporation of 0.25 wt.% of the ternary (ZnO-TiO<sub>2</sub>-SiO<sub>2</sub>) and quaternary (ZnO-TiO<sub>2</sub>-SiO<sub>2</sub>-CeO<sub>2</sub>) nanocomposites increased the membrane permeability of 377% and 329% respectively, compared with pure PES membrane. This could be explained by a drastic reduction of the contact angle values from 76° (pure PES membrane) to 32° (composites membranes). Moreover, the membranes prepared with various nanometric inorganic fillers displayed a lysozyme rejection higher than 96% (99% in the case of M-ZTS-Ce-0.25).

**Keywords:** Nanocomposite; Mixed matrix membrane (MMM); Polyethersulfone (PES); ZnO-TiO<sub>2</sub>-SiO<sub>2</sub>-CeO<sub>2</sub>

### 1. Introduction

In this decade, with the rapid development of membrane technology, considerable efforts were devoted to develop new membranes with improved performances [1]. In particular, membrane filtration using polymeric membrane is increasingly used in many industrial fields, including water and wastewater treatment processes, food and biotechnology industries [2–4]. Thus, polymeric membranes are usually cheaper than inorganic membranes, easy to produce and to handle. Among the different polymeric membrane materials, Polyethersulfone (PES) is one of most common polymer used for the synthesis of organic membrane, thanks to its good chemical and mechanical stability [5,6]. In order

to further improve the performance of PES membranes such as permeability and rejection ability, the membrane can be hybridized by incorporation of additives. In particular, hydrophilic additives are used to improve membrane permeability and anti-fouling properties while maintaining high rejection ability. The most popular hydrophilic additive is the Polyvinylpyrrolidone (PVP). However, PVP is easily oxidized in contact with oxidant chemicals, usually used for cleaning and disinfection steps after membrane fouling. Unfortunately, these oxidants accelerate the membrane ageing and PVP is known to be the weakest component of PES/PVP membranes [5]. Therefore, one alternative to PVP is to use organic (polymeric) membranes containing inorganic additives such as nanoparticles (so-called mixed

\* Corresponding author.

matrix membranes (MMM). During the MMM preparation, the nanoparticles used as membrane fillers can be of different natures including carbon based materials (carbon nanotubes, graphene oxide, fullerene), metal (oxide) based materials, metal organic frameworks [7–10]. Among these constituents, the use of nanoparticles of metal oxides was extensively considered. For example, ZnO, TiO<sub>2</sub>, SiO<sub>2</sub>, Al<sub>2</sub>O<sub>3</sub>, CeO<sub>2</sub> or ZrO<sub>2</sub> were used to improve the membrane properties such as permeability, fouling resistance ability, fouling reversibility or membrane mechanical strength [11,12]. Thus, the addition of metal oxide nanoparticles to the polymer matrix generally improves membrane hydrophilicity and might impact membrane structure and/or membrane charge. Several published studies focused on the addition of mono-metallic nanoparticles [2,8]. Other authors stressed the importance of using multi-metallic nanoparticles to improve the membrane performances [7]. Zhang et al. [13] reported a comparison between phosphorylated TiO<sub>2</sub>-SiO<sub>2</sub> (PTS)/polysulfone (PSF) composite membranes and other membranes such as PSF, SiO<sub>2</sub>/PSF and phosphorylated Zr-doped hybrid silica (SZP)/PSF (particle concentration 10 wt.%). They proved that PTS/PSF membrane exhibited higher performances than the other elaborated membranes. In fact, the non-stoichiometric PTS particles exhibited high hydrophilicity inherent to their composition favoring the occurrence of hydroxyl radical at their surface. In addition, Xu et al. [3] proved that the introduction of the composite N-doped graphene oxide (NRG)/TiO<sub>2</sub> in the structure of a PSF membrane greatly improved the hydrophilicity, permeability and antifouling properties, compared with the pure PSF membrane. In fact, the membranes exhibited an asymmetric structure with the homogenous dispersion of NRG/TiO<sub>2</sub> nanocomposites. They showed also that the permeability was dependent on the amount of NRG/TiO<sub>2</sub> nanocomposites blended (from 0.1% to 0.8% by weight of PSF membrane). This could be explained by the impact of the particles on membrane structure as the presence of particles led to the enlargement of the finger-like macrovoids within the membrane thickness. The fabricated membranes also exhibited high fouling resistance as the flux recovery ratio of the membranes increased from 65.3% (pure membrane) to 92.9%, and the irreversible fouling rate decreased to 7.6%, indicating that the water flux is highly recoverable. This was mainly due to the hydrophilic nature of the additive and a modification of the membrane roughness due to particles addition thus reducing the contact angle values of the MMM compared with the pure PSF membrane. Moreover, Zhang et al. [12] prepared a Ce-doped non-stoichiometric nanosilica/PSF composite membrane (particle concentration 10 wt.%). They demonstrated that SiO<sub>2</sub>/PSF membrane exhibited good performances in terms of hydrophilic properties, tensile strength and oil retention. The increased membrane hydrophilicity observed due to particles addition was attributed to the particles nature. In fact, non-stoichiometric inorganic oxide nanoparticles present many point defects on the inside and enough hydroxide radicals on the surface [12].

Additionally, a number of studies were dedicated to the preparation of PES-ceramic nanocomposites MMM. Thus, PES is widely used for membrane preparation as it exhibits excellent chemical and thermal resistances over a wide range of pH (from 2 to 12). On the other hand, PES is relatively

hydrophobic and thus require to be blended with hydrophilic compounds in order to improve both the properties and the performance of the membranes. In fact, several authors improved the permeability, the selectivity and the lifetime of PES membrane by intercalation of inorganic based nanomaterials such as Ti, Zr or ZnO nanoparticles [2,9,14].

However, to our knowledge, no information is available on both properties and performance of PES membranes containing ternary or quaternary composites as fillers. When incorporated into polymeric membranes, these particles are expected to increase the membrane hydrophilicity [12].

In this paper, the well known sol-gel method was used to prepare nanocomposites from the quaternary system ZnO-TiO<sub>2</sub>-SiO<sub>2</sub>-CeO<sub>2</sub> due to the high chemical and thermal stability of the selected oxides [15]. The obtained nanocomposites were subsequently used as fillers to fabricate new PES-nanocomposite MMM. Membranes with different amounts of fillers (0 to 0.5 wt.% of total solution) were prepared by the non-solvent induced inversion phase method. The physico-chemical properties of the obtained membranes were characterized. The filtration performances were studied in terms of membrane permeability and rejection ability.

## 2. Materials and methods

### 2.1. Chemicals for nanocomposite synthesis

The precursors used for nanocomposites synthesis: [Zn(NO<sub>3</sub>)<sub>2</sub>·6H<sub>2</sub>O], Ti[OCH(CH<sub>3</sub>)<sub>2</sub>]<sub>4</sub> and Si(OCH<sub>2</sub>CH<sub>3</sub>)<sub>4</sub> were supplied by Fluka (purity > 99%) and were used without further purification. Nanocomposites elaborated by solid-state reaction were obtained using silica (SiO<sub>2</sub>, Aldrich, Germany, 15 nm, purity > 99.8%), titania (TiO<sub>2</sub>, Aldrich, Germany, 20 nm, purity > 99.5%) and zinc oxide (ZnO, Aldrich, Germany, 90 nm, purity > 99.6%) powders supplied by Sigma-Aldrich (Germany).

### 2.2. Nanocomposite synthesis

This section describes the experimental routes used for composite synthesis. Sol-gel method was used to synthesize ZnO-SiO<sub>2</sub> (ZS) and TiO<sub>2</sub>-SiO<sub>2</sub> (TS) binary nanocomposites as well as ZnO-TiO<sub>2</sub>-SiO<sub>2</sub> (ZTS) ternary and ZnO-TiO<sub>2</sub>-SiO<sub>2</sub>-CeO<sub>2</sub> (ZTS-Ce) quaternary nanocomposites. Furthermore, a solid state reaction was also carried to elaborate a ZnO-TiO<sub>2</sub>-SiO<sub>2</sub> (zts) ternary nanocomposite, which was considered as a reference. Characteristics of ceramic composites are summarized in Table 1.

#### 2.2.1. Synthesis of ZnO-SiO<sub>2</sub> (ZS) and TiO<sub>2</sub>-SiO<sub>2</sub> (TS) nanocomposites

ZnO-SiO<sub>2</sub> (ZS) and TiO<sub>2</sub>-SiO<sub>2</sub> (TS) were prepared by a sol-gel process with a molar ratio of Zn/Si and Ti/Si of 1:1. In a typical experimental route, tetraethyl orthosilicate (TEOS) (Si(OCH<sub>2</sub>CH<sub>3</sub>)<sub>4</sub>) was mixed with ethanol (C<sub>2</sub>H<sub>5</sub>OH), distilled water, and nitric acid (HNO<sub>3</sub>) under stirring for 1 h. Then, aqueous solutions of zinc nitrate hexahydrate (Zn(NO<sub>3</sub>)<sub>2</sub>·6H<sub>2</sub>O) for ZnO-SiO<sub>2</sub> and Ti[OCH(CH<sub>3</sub>)<sub>2</sub>]<sub>4</sub> for TiO<sub>2</sub>-SiO<sub>2</sub> were added into the above solution of silica precursor under stirring for 1 h. The reaction was performed at room

temperature. The prepared samples were aged for 24 h to ensure the complete dispersion of the precursors and the homogenization of the solution. Finally, the samples were evaporated, dried at 60°C and sintered at 1,200°C for 2 h in air.

### 2.2.2. Synthesis of ZnO-TiO<sub>2</sub>-SiO<sub>2</sub> (ZTS) and ZnO-TiO<sub>2</sub>-SiO<sub>2</sub>-Ce (ZTS-Ce) nanocomposites

ZnO-TiO<sub>2</sub>-SiO<sub>2</sub> nanocomposite with a Zn/Ti/Si molar ratio of 1:1:2 was prepared by sol-gel process. Firstly, TEOS was mixed with ethanol (C<sub>2</sub>H<sub>5</sub>OH), distilled water and nitric acid (HNO<sub>3</sub>) under stirring for 1 h. Then, an aqueous solution of Zn(NO<sub>3</sub>)<sub>2</sub>·6H<sub>2</sub>O was added into the above solution under stirring for 1 h. The reaction was performed at room temperature. At the same time, TEOS was mixed with ethanol (C<sub>2</sub>H<sub>5</sub>OH), distilled water and nitric acid (HNO<sub>3</sub>) under stirring for 1 h. Then, an aqueous solution of Ti[OCH(CH<sub>3</sub>)<sub>2</sub>]<sub>4</sub> was added into the above solution under stirring for 1 h. Secondly, the two solutions were mixed and stirred for 1 h. In the case of ZTS-Ce sample, 3 mol% of ammonium cerium nitrate [(NH<sub>4</sub>)<sub>2</sub>Ce(NO<sub>3</sub>)<sub>6</sub>] was added to the solution. Then, the obtained mixture was aged for 24 h. The reaction was performed at room temperature. Finally, the samples ZTS and ZTS-Ce were evaporated, dried at 60°C and sintered at 1,200°C for 2 h in air. For ZTS sample elaborated by solid-state reaction (further called zts in this paper), 25 mol% ZnO, 25 mol% TiO<sub>2</sub> and 50 mol% SiO<sub>2</sub> powders were mixed

with absolute ethanol in an agate mortar. After milling these powders, during at least 1 h, the mixture was dried at 80°C/24 h. Cylindrical tablets (6 mm of diameter and 2 mm of thickness) obtained by uniaxial compaction until 150 MPa at the ambient temperature (25°C) were burned out at 500°C/4 h in air, then sintered in flowing argon at 1,200°C/2 h. The heating and cooling rates of the temperature were 10°C min<sup>-1</sup> and 20°C min<sup>-1</sup>, respectively. In the case of a powder sample analyze, the sintered tablet was crushed again with an agate mortar during 30 min.

### 2.3. Membrane elaboration

Hybrid membranes were fabricated by the wet phase inversion technique. The name and composition of all the prepared membranes are given in Table 2. Solutions were prepared for incorporating the desired amount of PES (Veradel 3000 MP, Solvay) and nanocomposites in N-Methyl-2-pyrrolidone (NMP, purity of 99.5%, Sigma-Aldrich, Germany). The obtained suspension was stirred for 16 h (500 rpm) at room temperature until the polymer was completely dissolved. Subsequently, the colloidal suspension was ultrasonicated for 30 min to remove eventual bubbles and to facilitate the nanocomposite dispersion. For all tested conditions, the PES concentration was 25 wt.% (total dope solution mass) while the nanocomposite concentration was adjusted to 0.25 or 0.5 wt.%. These low values of

Table 1  
Characteristics of ceramic nanocomposites

Codes	ZnO (mol%)	TiO <sub>2</sub> (mol%)	SiO <sub>2</sub> (mol%)	CeO <sub>2</sub> (mol%)	Specific area <sup>a</sup> S <sub>BET</sub> (m <sup>2</sup> g <sup>-1</sup> )	Pore diameter <sup>a</sup> (nm)	Porosity <sup>a</sup> (%)
TS	0	50	50	0	215	6.1	2.8
ZS	50	0	50	0	80	3.3	3.5
ZTS	25	25	50	0	465	7.8	3.2
zts	25	25	50	0	10	8.6	5.4
ZTS Ce	25	25	47	3	685	8.3	3.6

<sup>a</sup>Determined by BET method (estimated error 0.5%).

Table 2  
Dope solutions composition

Membrane name	PES concentration (wt.%)	Nanocomposite concentration (wt.%)	NMP concentration (wt.%)
M-PES	25.00	0.00	75.00
M-ZS-0.25	25.00	0.25	74.75
M-ZS-0.50	25.00	0.50	74.50
M-TS-0.25	25.00	0.25	74.75
M-TS-0.50	25.00	0.50	74.50
M-ZTS-0.25	25.00	0.25	74.75
M-ZTS-0.50	25.00	0.50	74.50
M-zts-0.25	25.00	0.25	74.75
M-zts-0.50	25.00	0.50	74.50
M-ZTS Ce-0.25	25.00	0.25	74.75
M-ZTS Ce-0.50	25.00	0.50	74.50

concentration were chosen to facilitate homogenous dispersion of the nanocomposite within the membrane matrix and to limit the risk of particle aggregation. In addition, the literature study showed that the incorporation of such low concentrations of metals or metal oxides based nanoparticles into the membrane matrix is efficient to improve filtration performances (Table 3). Pure PES solutions (without nanocomposite) were also synthesized as a reference. Thereafter, the obtained homogeneous suspension was cast uniformly (automatic film applicator; K4340, Elcometer) onto a non-woven polypropylene Viledon FO 2471 support (Freudenberg, Germany) attached onto a glass plate. The cast film thickness was set at 250  $\mu\text{m}$  while the casting speed and casting plate temperature were equal to 20  $\text{mm s}^{-1}$  and 28°C, respectively. The relative humidity was constant and equal to 60%. Then, the glass plate was instantly immersed into a non-solvent (deionized water) coagulation bath for 5 min at 20°C. Finally, the resulting membranes were stored in deionized water for at least 24 h before use.

#### 2.4. Nanocomposites and membranes characterization

##### 2.4.1. X-ray diffraction

X-ray diffraction (XRD) patterns were obtained with  $\text{CuK}\alpha$  radiation ( $\lambda = 1.5406 \text{ \AA}$ ) using a PHILIPS-PANALYTICAL (Netherlands); X'PERT pro MPD diffractometer at room temperature. The crystallite size of the sample was estimated from the Scherer equation:

$$D = \frac{(0.9\lambda)}{(B \cos\theta)} \quad (1)$$

where  $D$  is the crystallite size in  $\text{\AA}$ ,  $\lambda$  is the wavelength of the X-ray ( $\lambda = 1.5406 \text{ \AA}$ ),  $\theta$  is the Bragg angle in degrees, and  $B$  is the full width at half maximum (FWHM) of diffraction peaks, measured graphically in radians.

##### 2.4.2. Raman spectroscopy

The Raman scattering measurements were carried out using a 100/S-Bruker Raman Fourier Spectrometer. The 1.06 mm line of Nd-YAG laser was used for excitation with output laser power 100 mW.

##### 2.4.3. Scanning electron microscopy

The morphology analysis of both the nanocomposites and membranes was performed by using a scanning electron microscope (SEM, JEOL JSM 7100F, Japan) equipped with a link energy dispersive X-ray system (EDX). The samples were coated with gold before investigation. Cross-sectional views of the membranes were obtained after breaking the membranes in liquid nitrogen to preserve the membrane structure.

##### 2.4.4. Transmission electron microscopy

The nanocomposites were also characterized using transmission electron microscopy (TEM) (HR-TEM, JEM-3000F, JEOL Ltd. in Tokyo, Japan) operating at an accelerating voltage of 200 kV. Elemental mapping was conducted using a TEM equipped with an EDX.

Table 3  
Comparison to literature results relative to PES-ceramic nanoparticles mixed matrix membranes

Membrane	M-PES-Cu(tpa)@GO [1]	M-PES-SBA15-Ti M-PES-SBA15-Zr [2]	M-PES-GO-TiO <sub>2</sub> [3]	M-PES-ZnO [3]	M-PES-TiO <sub>2</sub> -SiO <sub>2</sub> [13]	M-PS-Ce-SiO <sub>2</sub> [12]	Present work
Particle concentration (wt.%)	0.5–1	0.3–0.6	0.1–0.8	0.5–5	10	10	0.25–0.50
Contact angle (Degree)	16–84	48–65	61–88	57–70	45.5–78	41.7–78.6	32–69
Permeability Lp (L h <sup>-1</sup> m <sup>-2</sup> bar <sup>-1</sup> )	51–85	318–650	120–233	20.28–41.22	116	22–24	2.19–8.26
Effluent type	Anionic dyes (Congo Red - Methyl Orange)	-	Bovine Serum Albumin BSA (5g/L)	River water/humic acid	Wastewater containing oil	Wastewater containing oil	Lysozyme
Retention percent (%)	80–90 (Congo Red) 40–60 (Methyl Orange)	-	92.5	96.8	92	98.3–98.8	96.0–98.8

#### 2.4.5. Brunauer–Emmett–Teller (BET) measurement

Specific surface area was measured using ASAP 2010 and TriStar 3020 micrometrics by adsorption of nitrogen at 77 K. Prior to adsorption measurements, the samples were degassed under vacuum of 20.8 Pa at 125°C for 30 min.

#### 2.4.6. Contact angle measurement

Contact angle tests were performed at room temperature using the surface energy evaluation system KRÜSS DROP SHAPE ANALYZER (Germany) – DSA30R (OCA) equipped with video capture. Contact angles of deionized water (H<sub>2</sub>O) were measured by depositing a sessile drop (1 µL) on the sample. Contact angle values were estimated as the tangent normal to the drop at the intersection (to the right and to the left) between the sessile drop and the surface. Images were taken within 30 s of the drop deposition. The reported contact angle values are the average of at least four measurements at different spots of the surface of the membrane.

#### 2.4.7. Streaming current measurements

Membrane surface electrokinetic properties were determined thanks to tangential streaming current measurements (Surpass 3, Anton Paar GmbH, Austria). Prior to the experiments, membrane samples were soaked overnight into the measuring solution (0.001 M KCl). Two identical rectangular membrane samples (2 cm × 1 cm) were then cut and fixed on sample holders using double-sided adhesive tape. The distance between the samples was set to 100 ± 5 µm for all measurements to allow the proper circulation of the measuring solution. The streaming current generated along the membrane surfaces was measured with Ag/AgCl electrodes for pressure ramps of 400 mbar. All measurements were performed at room temperature (19°C ± 1°C). The zeta potential was inferred from the standard Smoluchowski equation.

### 2.5. Filtration performance

#### 2.5.1. Pure water flux measurement and permeability determination

The permeability was evaluated by means of a dead-end filtration cell (XFUF07601, Merck, Germany). A circular piece of the prepared membrane was cut (76 mm effective diameter, 45.3 cm<sup>2</sup> effective areas) and inserted into the filtration cell. The cell was then filled with deionized water and pressurized using a nitrogen source in order to create the transmembrane pressure (permeate side at atmospheric pressure). The permeate produce in a given time was recovered in a beaker and weighed allowing the calculation of the permeate flux ( $J_v$ ) expressed in L h<sup>-1</sup> m<sup>-2</sup>. This protocol was repeated for several transmembrane pressure values in the range 0 to 4 bar. The slope of the straight line obtained by plotting the permeate flux as a function of the transmembrane pressure applied ( $\Delta P$  (bar)) thus corresponds to the membrane permeability ( $L_p$  in L h<sup>-1</sup> m<sup>-2</sup> bar) as shown in Eq. (2). All filtration tests were carried out at 20°C.

$$J_v = L_p \times \Delta P \quad (2)$$

where  $J_v$  is the permeate flux (L h<sup>-1</sup> m<sup>-2</sup>),  $L_p$  the membrane permeability (L h<sup>-1</sup> m<sup>-2</sup> bar<sup>-1</sup>) and  $\Delta P$  the transmembrane pressure (bar).

#### 2.5.2. Retention rate of the prepared membranes

Besides the membrane permeability, the efficiency of a membrane is particularly characterized by its ability to retain targeted species present in the feed solution. The retention rate represents the amount (expressed in %) of species retained by the membrane compared with that initially present in the feed solution, which can be calculated as follow:

$$R(\%) = \left( 1 - \frac{C_p}{C_0} \right) \times 100 \quad (3)$$

where  $C_0$  is the solute concentration of the feed solution (g L<sup>-1</sup>) and  $C_p$  the solute concentration of the permeate (g L<sup>-1</sup>). In this study, the protein retention was evaluated using lysozyme from hen egg (MW = 14.300 g mol<sup>-1</sup>, pI = 10.7) provided by Liot (purity: 92%, France) in hydrochloride form. Lysozyme was selected as it can be considered as a rigid protein (not easily deformable) [16] and thus is known to maintain its structure during membrane filtration [17]. Solutions of lysozyme in deionised water at a concentration of 1 g L<sup>-1</sup> (pH<sub>natural</sub> = 4) were prepared and used for the retention tests. Filtration runs were performed with the frontal filtration device described previously at constant transmembrane pressure of 3 bars. Lysozyme concentration, in the feed and permeate solutions was determined by UV spectroscopy (JASCO V-630) at 280 nm (absorption of the tryptophan contained in the lysozyme protein) according to the well-known Beer-Lambert law.

## 3. Results and discussion

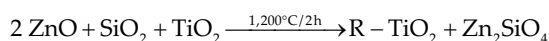
### 3.1. Nanocomposite characterization

As shown in Table 1, it is clear that the samples elaborated by sol-gel method display higher density than that obtained by classic solid-state reaction from nanopowders. However, all the samples present porosity lowers than 6%, confirming the good conditions of nanocomposite elaboration.

Fig. 1 shows the XRD patterns of the composites. XRD pattern of ZS shows the presence only of Zn<sub>2</sub>SiO<sub>4</sub> (Z<sub>2</sub>S) willemite phase (Rhombohedral structure, 00-037-1485). On the other hand, XRD pattern of TS reveals the presence of two forms of TiO<sub>2</sub>, rutile (tetragonal structure, 01-072-1148) and anatase (tetragonal structure, 01-071-1166) phases. The stronger peaks correspond to the rutile phase. No significant difference is observed between XRD pattern of ZTS obtained by sol-gel route and XRD pattern of zts elaborated by solid state reaction. The two ceramics are mainly composed of willemite Z<sub>2</sub>S phase (rhombohedral structure, 00-008-0492) and rutile TiO<sub>2</sub> phase (tetragonal structure, 01-072-1148). XRD pattern of ZTS Ce shows the presence of CeO<sub>2</sub> phase besides willemite Z<sub>2</sub>S phase (rhombohedral structure, 00-008-0492) and rutile TiO<sub>2</sub> phase. No peaks of SiO<sub>2</sub> or ZnO are detected, indicating the high reactivity of raw powders. This hypothesis could be justified by

the nanometric size of the particles of departure (10 nm for SiO<sub>2</sub> and 90 nm for ZnO) [18]. In order to confirm the XRD results, laser Raman Spectroscopy was used to investigate the phase composition of elaborated ceramics. Fig. 2 shows the Raman spectra of TS, ZS, ZTS, zts and ZTS Ce nanocomposites in the Raman Shift range of 100–1,000 cm<sup>-1</sup>. Wide peaks with low intensities, relative to anatase phase (A-TiO<sub>2</sub>) were detected at 400 and 516 cm<sup>-1</sup> for TS sample only, in good agreement with XRD results [16,19,20]. Other intense peaks corresponding to rutile phase (R-TiO<sub>2</sub>) were observed at 145, 240, 450 and 610 cm<sup>-1</sup> for all nanocomposites (except ZS, as expected) [16,19,20]. Furthermore, the characteristic peaks of Z<sub>2</sub>S [16,19,20] located at 875, 912 and 953 cm<sup>-1</sup>, were detected for all the samples with the exception of TS composite.

The new phases obtained by sintering the mixture (ZnO-TiO<sub>2</sub>-SiO<sub>2</sub>) at 1,200°C/2 h could be explained according to the following reaction:



Furthermore, based on XRD results, the crystallite sizes of TiO<sub>2</sub> rutile (R-TiO<sub>2</sub>) and Z<sub>2</sub>S were estimated by using the Scherer equation. According to the peaks located at 27.45° for R-TiO<sub>2</sub> and 34.23° for Z<sub>2</sub>S, the crystallite size values of R-TiO<sub>2</sub> were 32.5, 39.5, 41.5 and 43.5 nm in TS, ZTS, zts and ZTS Ce, respectively. The estimated error was about 2%. Furthermore, the crystallite size values of Z<sub>2</sub>S were 43.1, 40.4, 40.5 and 40.6 nm in ZS, ZTS, zts and ZTS Ce, respectively. It is clear that rutile crystallite size depends slightly on the ceramic composition, whereas, Z<sub>2</sub>S crystallite guards the same size in the ternary system ZnO-TiO<sub>2</sub>-SiO<sub>2</sub>.

In order to confirm these results and further assess the composition and morphology of the samples, SEM-EDX analyses were performed. Fig. 3 shows SEM images of TS (a), ZS (b), ZTS (c), zts (d) and ZTS Ce (e) composites. An example of EDX analysis relative to ZTS Ce sample is shown in Fig. 4. The main phases shown by SEM analysis are in agreement with XRD and Raman results. As confirmed by EDX analysis,

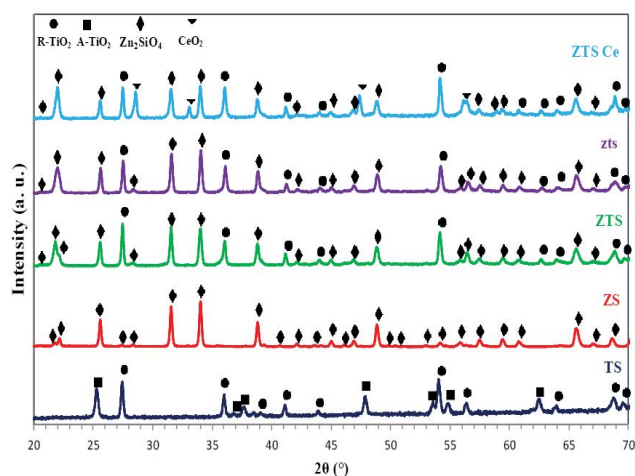


Fig. 1. XRD patterns of TS, ZS, ZTS, zts and ZTS Ce composites sintered at 1,200°C/2 h.

very small rutile grains (R-TiO<sub>2</sub>) with size less than 100 nm are present in TS, ZTS, zts and ZTS Ce samples. However, Zn<sub>2</sub>SiO<sub>4</sub> (Z<sub>2</sub>S) grains are assembled in spherical aggregates of about 1 μm of diameter. Nanoceria (50 nm) is also detected in ZTS Ce sample.

Fig. 5 shows TEM images of TS (a), ZS (b), ZTS (c), zts (d) and ZTS Ce (e) composites. Spherical nanosized (less than 100 nm) grains are observed, confirming the nanometric scale of all the composites. Except for ZS nanocomposite (b), all the other materials contain at least two nanometric phases, as confirmed also by SEM analysis. In addition, it seems that the size of zts sample (elaborated by classical solid state reaction) estimated by SEM and TEM micrographs is higher than ZTS (obtained by sol-gel route) diameter. Besides, ZTS material is less porous than zts composite (Table 1). For these expected reasons, two different methods were used to elaborate the composites. It is well known that sol gel technique gives better homogeneity with smaller grain size and lower porosity [18].

### 3.2. MMM characterization

Side-view SEM micrographs of the fabricated membranes are shown in Fig. 6. All the obtained membranes were asymmetric and exhibited finger-like macrovoids structure suggesting that nanocomposite addition within the polymer matrix does not drastically modify the membrane macrostructure. Unfortunately, the nanocomposite presence could not be detected on this side views. However, this finding is not surprising taking into account the extremely low amount of particle added into the polymer solution.

Contact angle measurement is an important indicator for membrane hydrophobicity or hydrophilicity. A lower contact angle indicates the higher hydrophilicity of the membrane. The membranes with higher surface hydrophilicity will in general have a greater ability to attract water molecules and thus reduce the adsorption of contaminants, which would play a positive role in improving membrane permeability and membrane antifouling ability. Fig. 7 shows the results of the contact angle measurements for both the pure PES membrane and MMM. The pure PES membrane

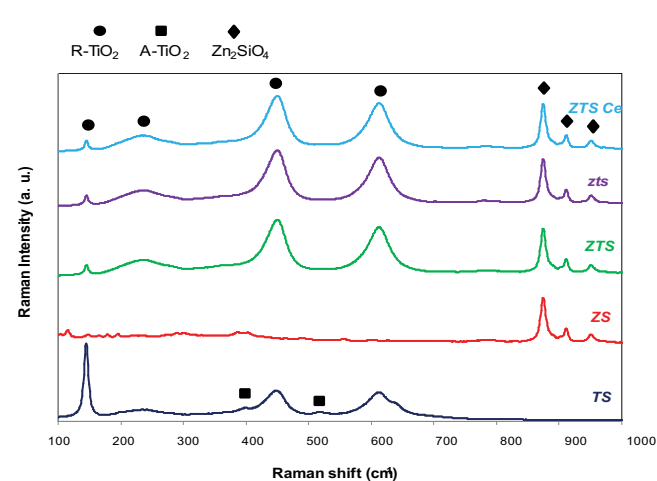


Fig. 2. Raman spectra of TS, ZS, ZTS, zts and ZTS Ce composites sintered at 1,200°C/2 h.

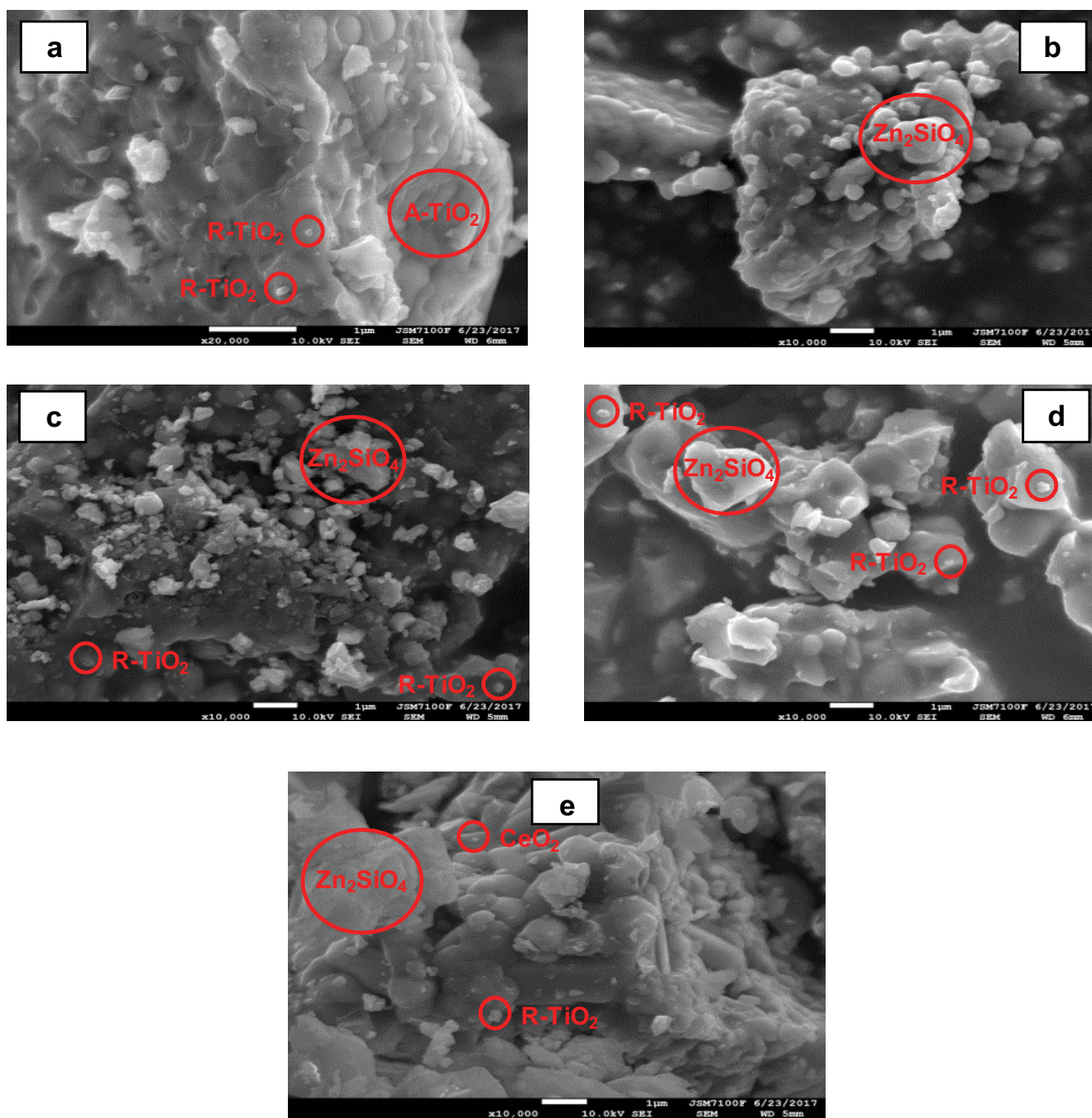


Fig. 3. SEM micrographs of TS (a), ZS (b), ZTS (c), zts (d) and ZTS Ce (e) sintered at 1,200°C/2 h.

shows a water contact angle of 76° due to relatively hydrophobic nature of the PES. In comparison, the water contact angles of the MMM are in the range 32° to 69° thus indicating the positive effect of nanocomposites addition on membrane hydrophilicity (whatever the nanocomposite composition). This could be explained by the occurrence of many hydrophilic hydroxide radicals on the surface of inorganic oxide nanoparticles [21]. According to the contact angle measurements, the most hydrophilic membranes are those made of ZTS nanocomposite followed by ZTS Ce and TS. On the other hand, the membranes incorporated with

zts and ZS nanocomposites are more hydrophobic. It is worth noting that zts and ZS nanocomposites are also the ones exhibiting the lower specific area (10 and 80 m<sup>2</sup> g<sup>-1</sup>; Table 1). On the other hand, TS, ZTS and ZTS Ce exhibit much larger surface area higher than 200 m<sup>2</sup> g<sup>-1</sup>. In particular, ZTS Ce has the higher surface area (685 m<sup>2</sup> g<sup>-1</sup>). This result could be explained by the presence of third CeO<sub>2</sub> phase which prevents magnification of the main components (R-TiO<sub>2</sub> and Zn<sub>2</sub>SiO<sub>4</sub>) of the material. Additionally, for the two ternary composites, ZTS displays higher specific area (465 m<sup>2</sup> g<sup>-1</sup>) than zts sample (10 m<sup>2</sup> g<sup>-1</sup>). This difference

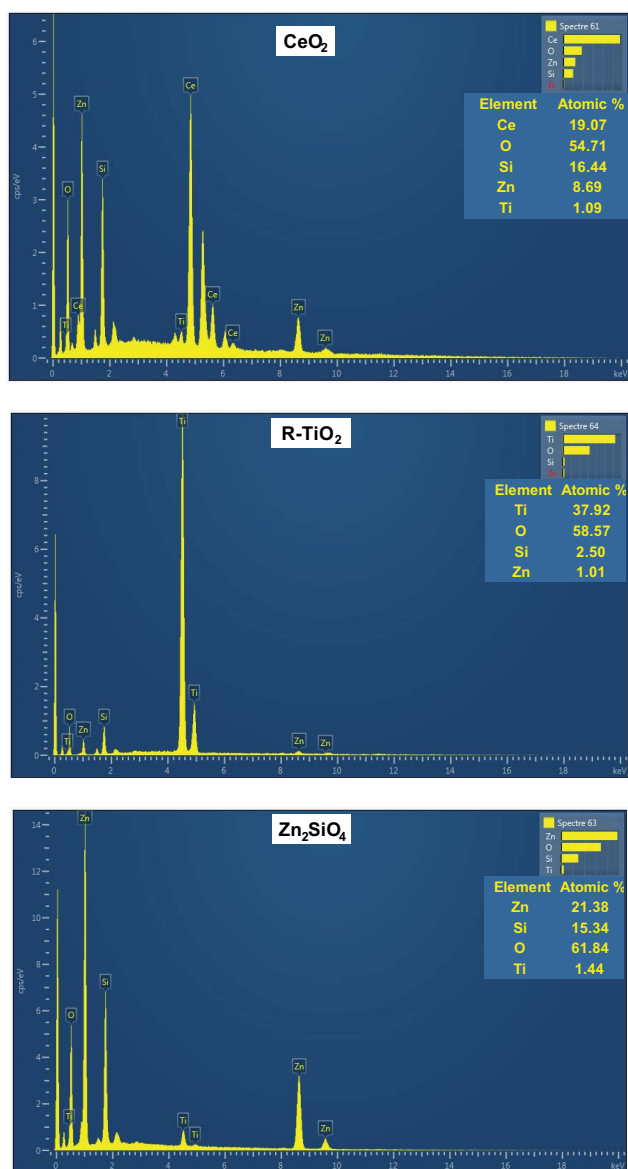


Fig. 4. EDX maps of ZTS Ce sintered at 1,200°C/2 h.

could be attributed to the elaboration process since sol-gel route allows obtaining homogenous composite with higher density (porosity < 6%) and smaller grains. These differences of surface area could be related to difference on the size of the nanocomposites. The higher the surface area is the lower the particle diameter. At the end, difference in particle diameter might affect membrane hydrophilicity as several parameters such as particles size, shape or tendency to aggregation are known to affect membrane properties [22–26]. Furthermore, it can be observed that, for a given nanocomposite type, the better values of contact angle are obtained for the membranes having a nanocomposite loading of 0.25 wt.% and not in the case of the higher particle concentration (0.50 wt.%). Such behavior was also observed for other PES membranes blended with inorganic nanoparticles even at low amounts (Table 3). In particular, Balta et al. [27] showed that the addition of ZnO particles into the

membrane matrix drastically reduced the contact angle values (from 70° to 35°) even at extremely low concentration (0.035 wt.%). The contact angle values were independent on particles concentration up to 0.25 wt.% but slightly increased in the concentration range 0.25 to 1.00 wt.%. Thus, an increase in particle loading can lead to a less homogeneous dope suspension due to particle aggregation (even for particle concentration lower than 1.00 wt.%) which impair membrane hydrophilicity [28]. Taking into account the nanocomposite nature and concentration, the best hydrophilicity is observed for the M-ZTS-0.25 membrane with a very low contact angle value of 32° followed by the M-ZTSCe-0.25 (39°) and M-TS-0.25 (44°) membranes. Interestingly, M-ZTS-0.25 and M-ZTS Ce-0.25 exhibit contact angle values below 40° much lower than obtained in studies gathered in Table 3 (except for PES membrane incorporating Cu(tpa)@GO particles [1]) thus indicating their superior hydrophilic properties. In fact, SEM analysis showed that ZTS and ZTS Ce samples are distinguished by a more uniform phase distribution and better homogeneity (Fig. 3). These reasons contribute to improve the hydrophilic nature of ZTS and ZTSCe composites presenting more hydroxide radicals on the surface.

Membrane surface charge was determined in terms of zeta potential thanks to tangential streaming potential measurements. It is known as an important factor to evaluate membrane fouling ability by charged molecules. Fig. 8 shows the variation of the zeta potential for each membrane in the pH range from 2 to 5. For better clarity, the results were plotted in two different graphs for the membrane incorporated with 0.25 wt.% (a) and 0.50 wt.% (b). It can be observed that nanocomposite incorporation within the PES matrix has only marginal effect on the membrane isoelectric point (iep). Thus, whatever the nanocomposite nature, concentration and all membranes exhibits an iep of  $3.3 \pm 0.2$  except the M-ZTS Ce-0.25 and the M-ZTS-0.5 for which the iep values are 2.8 and 3.7 respectively. Furthermore, when considering the zeta potential values of the different membrane at pH 4 (pH of the solution to be filtered), all the membranes (with and without nanocomposites incorporated) are negatively charged and exhibit a moderate charge of about  $-15 \pm 5$  mV. It can be concluded from these observations that no major difference of surface charge exists for the different membranes synthesized in this study.

The pure water membrane permeability was determined for all MMM membranes (Fig. 9). Both concentration and nature of fillers incorporated in the solutions appear to have an impact on MMM permeability. Interestingly, whatever the nanocomposite type, membrane permeability is higher for a filler concentration of 0.25 wt.% compared with that of 0.50 wt.% (except for the M-ZS membranes). Previous studies, for other membrane fillers, also reported the existence of an optimal particle concentration on membrane filtration performance. In particular, an increasing concentration of filler might lead to its less efficient dispersion into the colloid thus leading the occurrence of particle aggregates that negatively affect the membrane permeability (even at low particle concentration below 1 wt.%) [27]. In addition, particle concentration is known to have a direct impact on membrane microstructure. In fact, for PES membranes blended with silica-based material, Guo et al. [2], showed that a particle concentration above 0.3 wt.% led

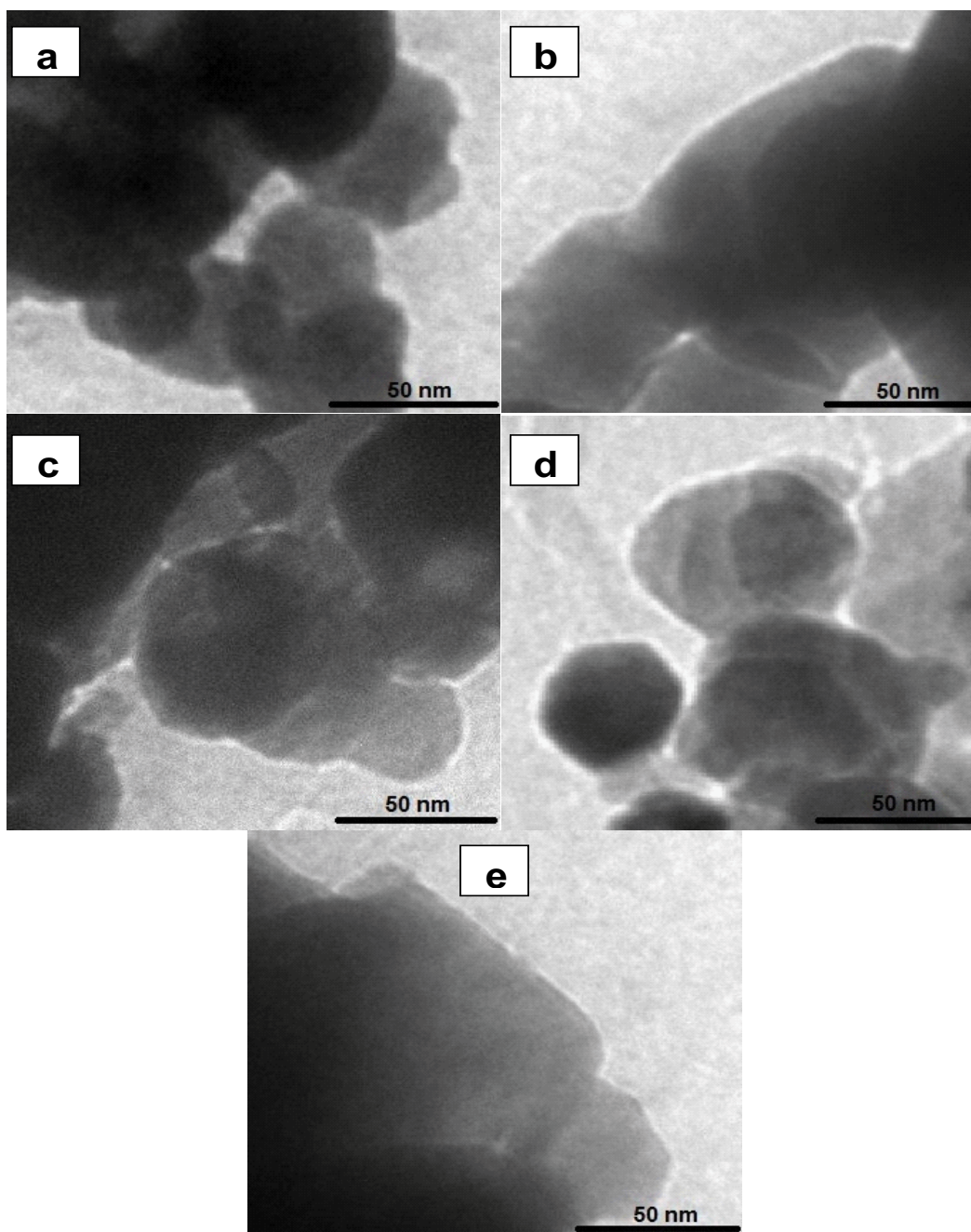


Fig. 5. TEM micrographs of TS (a), ZS (b), ZTS (c), zts (d) and ZTS Ce (e).

to an increase of the membrane skin layer thickness and a reduction of the occurrence of finger-like macro-voids compared with lower concentration. Such structure contributes to increase the material hydraulic resistance and thus has a detrimental effect on the membrane permeability [2]. Of course, this optimal concentration of fillers is highly dependent on the polymer/filler/solvent natures and properties but also on the operating conditions (membrane synthesis technique, polymer concentration, etc.) [29]. However, whatever the nanocomposite type, most of the elaborated membranes exhibit higher pure water permeability compared with the pure PES membrane. In particular, the

incorporation of 0.25 wt.% of the ternary ( $\text{ZnO-TiO}_2\text{-SiO}_2$ ) and quaternary ( $\text{ZnO-TiO}_2\text{-SiO}_2\text{-CeO}_2$ ) nanocomposites led to an important increase of the membrane permeability of 377% and 329% respectively, compared with the pure PES membrane. Furthermore, the M-TS membrane also shows promising permeability increase of 248%. In order to get more insights into this permeability increase due to particle addition in the polymeric solution, the membrane permeability was plotted against the membrane contact angle values (Fig. 10). From this figure, it can clearly be seen that the more permeable membranes are the ones having the lower values of contact angles. These results suggest that

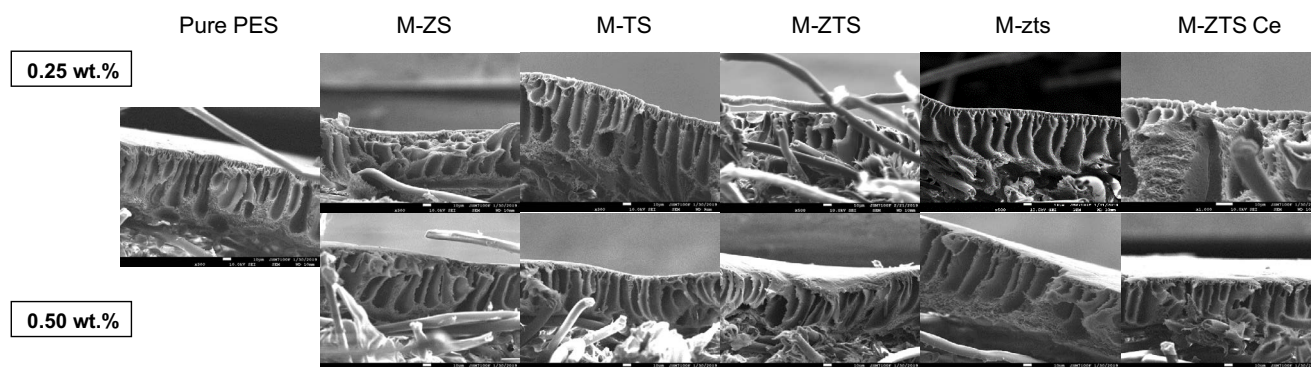


Fig. 6. Cross-section SEM micrographs of the pure PES membrane and MMM with filler concentration of 0.25 wt.% (top row) and 0.50 wt.% (bottom row). The presence of fibers on some images is due to the presence of the non-woven support.

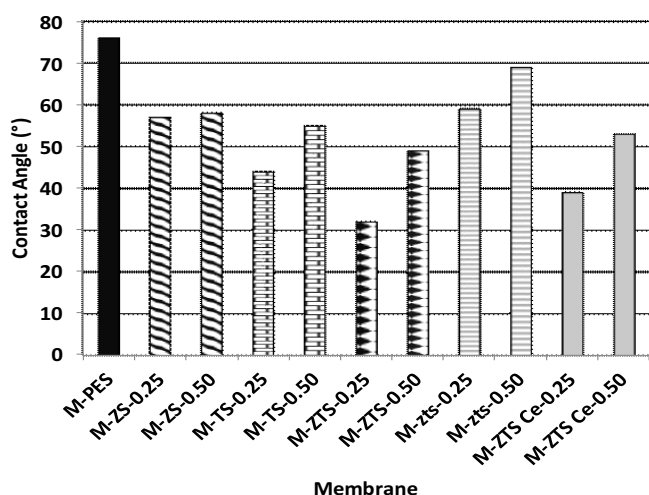


Fig. 7. Contact angle values of the different prepared membranes.

an increase in membrane hydrophilicity induced by the nanocomposite addition plays a key role in the increase of membrane permeability. Moreover, it has to be noted that, whatever the membrane composition (pure PES membrane or MMM), contact angle values higher than  $55^\circ$  led to low and constant permeability values of about  $2 \text{ L h}^{-1} \text{ m}^{-2} \text{ bar}^{-1}$ . The permeability values of our membranes are lower than those of membranes already developed by other authors in similar conditions (Table 3). This difference in permeability could be explained by the high density of our composites (porosity lower than 6%) and the low size of the pores (pore diameter lower than 10 nm). A notable exception is the M-zts-0.25 which has a contact angle value of  $59^\circ$  but permeability 2 times higher than the pure PES membrane. This observation indicates that, in the tested conditions, membrane hydrophilicity is not the only parameter influencing the pure water membrane permeability. In particular, modification of the membrane micro-structure due to particle presence could also impact filtration performance.

Lysozyme rejection rate was also evaluated for the different membranes (Fig. 11). The pure PES membrane allows a lysozyme rejection rate of 80%. Besides, the incorporation of nanocomposites into the polymer matrix leads to an

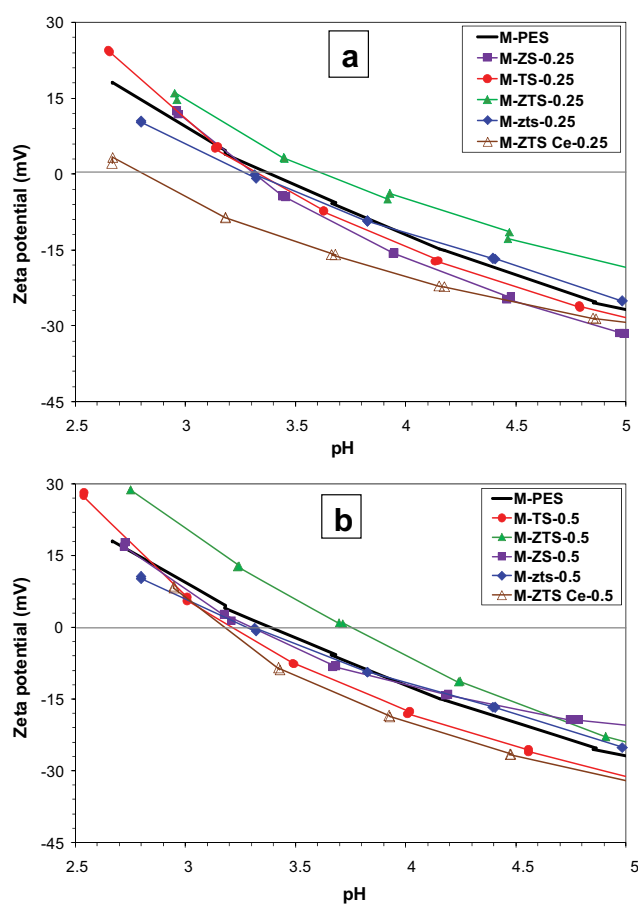


Fig. 8. Surface charge of the prepared membranes with filler concentration of 0.25 wt.% (a) and 0.50 wt.% (b).

important increase of the rejection, whatever the nature and concentration of the filler. In particular, the membrane incorporating ZST Ce nanocomposite allows a lysozyme rejection higher than 99%. However, membrane rejection rate seems to be dependent of the nanocomposite concentration. Thus, for all nanocomposites prepared by the sol-gel method, rejection is always higher at higher composite amount. To sum-up, the incorporation of nanocomposites into the membrane PES

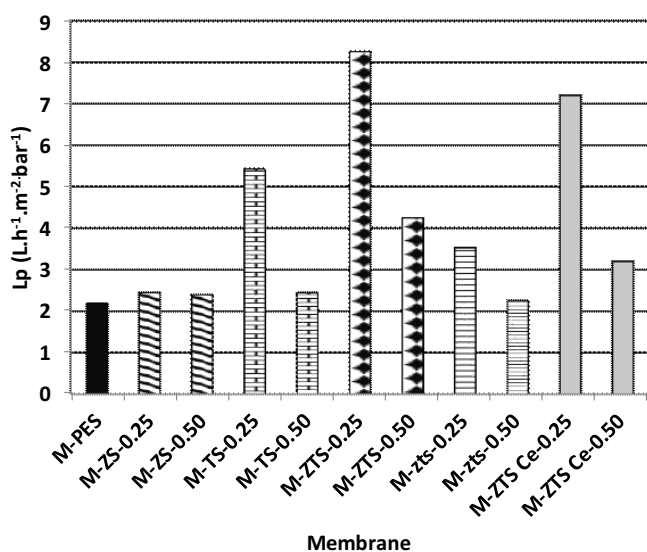


Fig. 9. Permeability of the prepared membranes.

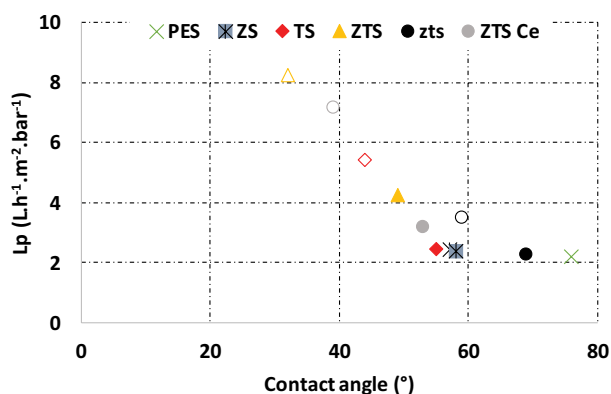


Fig. 10. Membrane permeability variation against contact angle values (empty symbols: filler concentration of 0.25 wt.%; full symbols: filler concentration of 0.50 wt.%).

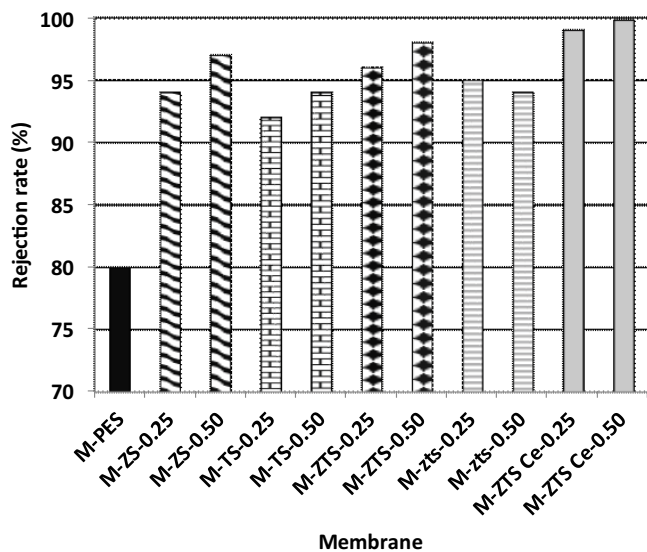


Fig. 11. Lysozyme rejection efficiency by the different membranes.

matrix allows to both improve the membrane permeability and rejection rate. In particular, the ternary (ZnO-TiO<sub>2</sub>-SiO<sub>2</sub>) and quaternary (ZnO-TiO<sub>2</sub>-SiO<sub>2</sub>-CeO<sub>2</sub>) nanocomposites allow to markedly increase the membrane permeability (up to 4 times in the best case) while obtaining rejections in the range of 96.0% to 99.8%. It has also to be noted that the highest membrane permeabilities are usually obtained for a nanocomposite concentration of 0.25 wt.% while the highest rejection rates are observed at the concentration of 0.50 wt.%. The rejection rate of the 0.25 wt.% membranes is only slightly lower than that of the 0.50 wt.% concentration. Finally, the M-ZST-0.25 and M-ZST-Ce-0.25 exhibits the higher performances with highly improved membrane permeability (more than 3.5 times, compared with pure PES membrane) while having high retention ability (99% in the case M-ZST-Ce-0.25). Although the effluent is not the same, the retention rate of our membranes is comparable to other works published by Xu and Zhang [3,12], but much higher than M-PES-TiO<sub>2</sub>-SiO<sub>2</sub> [13] tested with oil and M-PS-GO-TiO<sub>2</sub> tested with BSA solution [3].

#### 4. Conclusion

The design of advanced filtration membranes plays an important role in solving global water treatment problems. TS, ZS, ZTS, zts and ZTS Ce were incorporated in PES membrane. All nanocomposites were successfully prepared and fully characterized. The composites incorporated in the polymer matrix played a favorable role in the performance of the resulting membranes. Thus, these membranes exhibited superior performances compared with the pure PES membranes. The intercalation of nanocomposites enhanced both the permeability and retention ability of the membranes. In particular, the hydrophilicity of the composite membranes, which plays an important role in the permeation flow, was markedly increased for the best performing membranes.

#### Acknowledgments

The authors would like to thank the Solvay and Freudenberg companies for kindly providing the PES polymer and membrane support, respectively. Francis Gouttefangeas is acknowledged for SEM images and EDX analyses performed at CMEBA (ScanMAT, University of Rennes 1), which received a financial support from the European Union (CPER-FEDER 2007-2014).

François Cheviré is also acknowledged for XRD analyses.

#### References

- [1] T.A. Makhetha, R.M. Moutloali, Antifouling properties of cu(tpa)@go/pes composite membranes and selective dye rejection, *J. Membr. Sci.*, 554 (2018) 195–210.
- [2] J. Guo, A. Sotto, A. Martín, J. Kim, Preparation and characterization of polyethersulfone mixed matrix membranes embedded with Ti or Zr incorporated SBA-15 materials, *J. Ind. Eng. Chem.*, 45 (2017) 257–265.
- [3] H. Xu, M. Ding, S. Liu, Y. Li, Z. Shen, K. Wang, Preparation and characterization of novel polysulphone hybrid ultrafiltration membranes blended with N-doped GO/TiO<sub>2</sub> nanocomposites, *J. Polym.*, 117 (2017) 198–207.
- [4] M. Jonoobi, A. Ashori, V. Siracusa, Characterization and properties of polyethersulfone/modified cellulose nanocrystals nanocomposite membranes, *J. Polym. Test.*, 76 (2019) 333–339.

- [5] Y. Hanafi, P. Loulergue, S. Ababou-Girard, C. Meriadec, M. Rabiller-Baudry, K. Baddari, A. Szymczyk, Electrokinetic analysis of PES/PVP membranes aged by sodium hypochlorite solutions at different pH, *J. Membr. Sci.*, 501 (2016) 24–32.
- [6] B. Van der Bruggen, Chemical modification of polyethersulfone nanofiltration membranes: a review, *Appl. Polym. Sci.*, 114 (2009) 630–642.
- [7] J.H. Haveri, Z.V.P. Murthy, A comprehensive review on anti-fouling nanocomposite membranes for pressure driven membrane separation processes, *Desalination*, 379 (2016) 137–154.
- [8] S. Daer, J. Kharraz, A. Giwa, S.W. Hasan, Recent applications of nanomaterials in water desalination: a critical review and future opportunities, *Desalination*, 367 (2015) 37–48.
- [9] Y. Manawi, V. Kochkodan, M.A. Hussein, M.A. Khaleel, M. Khraisheh, N. Hilal, Can carbon-based nanomaterials revolutionize membrane fabrication for water treatment and desalination, *Desalination*, 391 (2016) 69–88.
- [10] X. Li, Y. Liu, J. Wang, J. Gascon, J. Li, B.V. Der Bruggen, Metal-organic frameworks based membranes for liquid separation, *Chem. Soc. Rev.*, 46 (2017) 7124–7144.
- [11] M. Pendergast, E.M.V. Hoek, A review of water treatment membrane nanotechnologies, *J. Energy Environ. Sci.*, (2011) 1946–1971.
- [12] Y. Zhang, L. Shan, Z. Tu, Preparation and characterization of novel Ce-doped non-stoichiometric nanosilica/polysulfone composite membranes, *Sep. Purif. Technol.*, 63 (2008) 207–212.
- [13] Y. Zhang, F. Liu, Y. Lu, L. Zhao, L. Song, Investigation of phosphorylated TiO<sub>2</sub>-SiO<sub>2</sub> particles/polysulfone composite membrane for wastewater treatment, *Desalination*, 324 (2013) 118–126.
- [14] A.L. Ahmad, A.A. Abdulkarim, Z.M.H. Mohd Shafie, B.S. Oi, Fouling evaluation of PES/ZnO mixed matrix hollow fiber membrane, *Desalination*, 403 (2017) 53–63.
- [15] B.A. Sava, T. Vişan, Raman and FTIR studies of some sol-gel based glasses in the ZnO-TiO<sub>2</sub>-SiO<sub>2</sub> system, *J. Sci. Bull. B*, 69 (2007) 1454–2331.
- [16] R. Ueberbacher, E. Haimer, R. Hahn, A. Jungbauer, Hydrophobic interaction chromatography of proteins: quantitative assessment of conformational changes, *J. Chromatogr. A*, 1198–1199 (2008) 154–163.
- [17] J. Belmejdoub, M. Rabiller-Baudry, D. Delaunay, G. Gésan Guiziou, Structural modifications of globular proteins in an ultrafiltration loop as evidenced by intrinsic fluorescence and reverse-phase liquid chromatography, *Sep. Purif. Technol.*, 96 (2012) 274–288.
- [18] A. Sedaghat, E. Taheri-Nassaj, G.D. Soraru, T. Ebadzadeh, A comparative study of microstructural development in the sol-gel derived alumina-mullite nanocomposites using colloidal silica and tetraethyl orthosilicate, *J. Sol-Gel Sci. Technol.*, 58 (2011) 689–697.
- [19] M. Schraml, T. Marth, K.L. Walther, A. Wokaun, Porous silica gels and TiO<sub>2</sub>/SiO<sub>2</sub> mixed oxides prepared via the sol-gel process: characterization by spectroscopic techniques, *J. Non-Cryst. Solids*, 143 (1992) 93–111.
- [20] M. Muzafa Jumidali, M.R. Hashim, K. Al-Heuseen, Analysis of the properties of germanium/zinc silicate film growth through a simple thermal evaporation technique for hydrogen gas sensing and deep UV photodetector application, *Mater. Sci. Semicond. Process.*, 16 (2013) 1360–1364.
- [21] J. Cho, M.S. Joshi, C.T. Sun, Effect of inclusion size on mechanical properties of polymeric composites with micro and nanoparticles, *Compos. Sci. Technol.*, 66 (2006) 1941–1952.
- [22] X. Cao, J. Ma, X. Shi, Z. Ren, Effect of TiO<sub>2</sub> nanoparticle size on the performance of PVDF membrane, *Appl. Surf. Sci.*, 253 (2006) 2003–2010.
- [23] V. Vatanpour, S. Siavash Madaeni, A.R. Khataee, E. Salehi, S. Zinadini, H.A. Monfared, TiO<sub>2</sub> embedded mixed matrix PES nanocomposite membranes: influence of different sizes and types of nanoparticles on antifouling and performance, *Desalination*, 292 (2012) 19–29.
- [24] L. Jinlong, Z. Deshuai, S. Guozhe, Z. Chunming, Z. Qigang, J. Lihua, Nanocomposite of Cu-TiO<sub>2</sub>-SiO<sub>2</sub> with high photoactive performance for degradation of Rhodamine B Dye in aqueous wastewater, *Nanosci. Nanotechnol.*, 12 (2012) 6265–6270.
- [25] H. Rajabi, N. Ghaemi, S. Madaeni, P. Daraei, B. Astinchap, S. Zinadini, S.H. Razavizadeh, Nano-ZnO embedded mixed matrix polyethersulfone (PES) membrane: Influence of nano-filler shape on characterization and fouling resistance, *Appl. Surf. Sci.*, 349 (2015) 66–77.
- [26] G. Calleja, D.P. Serrano, R. Sanz, P. Pizarro, A. Garci, Study on the synthesis of high-surface-area mesoporous TiO<sub>2</sub> in the presence of nonionic surfactants, *Ind. Eng. Chem. Res.*, 43 (2004) 2485–2492.
- [27] S. Balta, A. Sotto, P. Luis, L. Benea, B. Van der Bruggen, J. Kim, A new outlook on membrane enhancement with nanoparticles: the alternative of ZnO, *J. Membr. Sci.*, 389 (2012) 155–161.
- [28] Y.H. Teow, A.L. Ahmad, J.K. Lim, B.S. Ooi, Preparation and characterization of PVDF/TiO<sub>2</sub> mixed matrix membrane via in situ colloidal precipitation method, *Desalination*, 295 (2012) 61–69.
- [29] K.P. Kuo, M. Cheryan, Ultrafiltration of acid whey in a spiral-wound unit: effect of operating parameters on membrane fouling, *J. Food Sci.*, 48 (1983) 1113–1118.